We are IntechOpen,
the world's leading publisher of
Open Access books
Built by scientists, for scientists

6,900
Open access books available

185,000
International authors and editors

200M
Downloads

154
Countries delivered to

Our authors are among the

TOP 1%
most cited scientists

12.2%
Contributors from top 500 universities

CLARIVATE ANALYTICS

BOOK
CITATION
INDEX

INDEXED

WEB OF SCIENCE™

Selection of our books indexed in the Book Citation Index
in Web of Science™ Core Collection (BKCI)

Interested in publishing with us?
Contact book.department@intechopen.com

Use of Ionic Liquid Under Vacuum Conditions

Susumu Kuwabata, Tsukasa Torimoto,
Akihito Imanishi and Tetsuya Tsuda

1. Introduction

Ionic liquid (IL) is a kind of salt that can stay as a liquid phase even at room temperature. However, researchers sometimes prefer to call it room temperature ionic liquid (RTIL) to distinguish between liquid salt at around room temperature and that at high temperature. Fig. 1 shows structural formulas of well-known ILs with their names and abbreviations. The liquid possesses several attracting characteristics like high ionic conductivity, wide electrochemical windows, and negligible vapor pressure [1-5]. All features imply that IL has high stability and inertness, which have become very useful to utilize IL as electrolytes for Li-ion secondary batteries and PEM fuel cells, reaction solvents for organic synthesis and nanoparticle preparation, and lubricants usable in cosmic space [4].

The negligible vapor pressure of most ILs at room-temperature means that such the ILs can be put in a vacuum chamber without any vaporization. This fact invented a new technological concept because there are several instruments that require vacuum conditions for sample analyses and material manufacturing. Those instruments are basically designed for dealing with solid samples because it is quite common sense that the vacuum conditions should provide dry atmosphere. In other words, conventional procedures with such the instruments cannot be applied to any wet sample, although researchers frequently meet the cases where they would like to deal with wet samples and liquid itself in vacuum equipments. Possibility to introduce ILs to the vacuum instruments could innovatively change the techniques requiring vacuum conditions. Then, some researchers including our research group started to put ILs in vacuum chambers of several instruments.
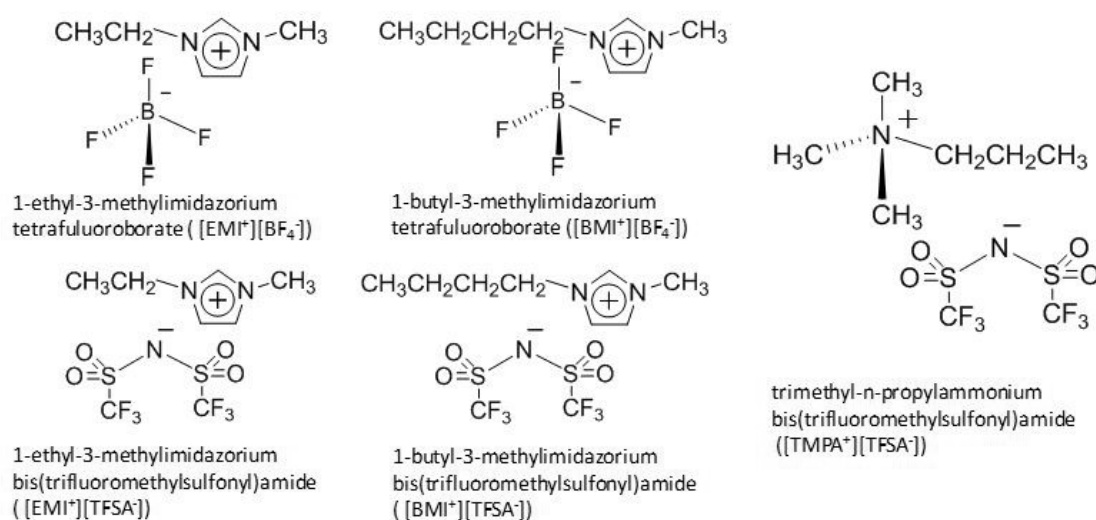
Figure 1. Structure formulas of typical ionic liquids with names and their abbreviations.

In this chapter, new techniques developed by putting ILs in the vacuum chambers of instruments will be introduced. Actually there are some other liquids having very low vapor pressure like silicon grease, which also can be introduced into the vacuum chamber. However, such oily medias cannot work as solvent for chemical and physical reaction because of their extremely high viscosity. On the other hand, ILs, which work well as solvent and electrolyte, make the dry vacuum conditions become wonderful wet world as will be introduced in this chapter.

2. XPS analysis

XPS is an instrument for analyzing the composition of solid materials and chemical state of each element. To detect generated photoelectrons with high sensitivity, vacuum condition is required. This condition is also effective for avoiding contamination of the sample surfaces. Although many researchers would like to put liquid into this instrument, vacuum condition in its sample chamber does not allow it. Nevertheless, some papers have reported the aggressive attempt to analyze the liquid surface by XPS with intricately designed sample stages [6-9]. In contrast, IL that is not vaporized under ultra-vacuum conditions can easily be put in the XPS chamber without any specific technique of modification.

$[EMI^+][C_2H_5SO_3{}^-]$ was the first IL that has been subjected to XPS analyses. It was found that IL emitted stable photoelectron flux, giving XPS spectra with high resolution [10-13]. Then, the obtained spectra enable a peak separation by the fitting calculations. Figure 2(a) shows the C1s spectrum of $[EMI^+][C_2H_5SO_3{}^-]$ together with the fitting curves based on C elements in five locations in the IL [14]. The XPS analysis of IL also allows detection of species dissolved in the IL, enabling in situ analysis of chemical reactions. An example is shown in Fig. 2(b) which

were XPS spectra of $Pd(OAc)_2(PPh_3)$ dissolved in $[EMI^+][C_2H_5SO_3^-]$ [14]. Successive measurements showed that the intensity of spectra due to Pd(II) decreased, while the spectra due to Pd^o increased, showing decomposition of Pd complex known as the Heck catalyst.

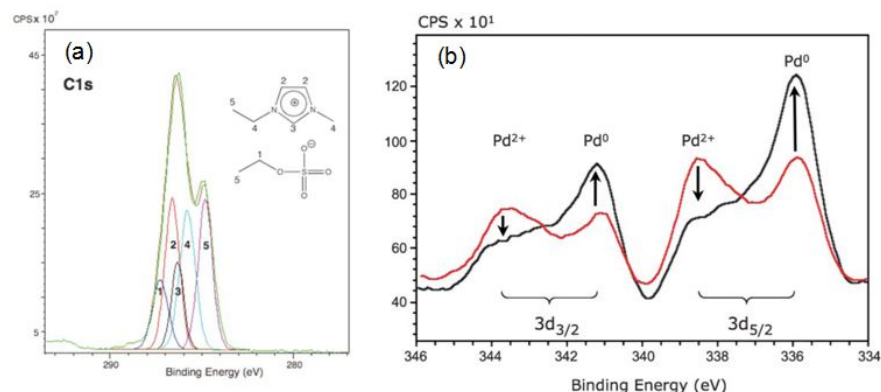**Figure 2.** High resolution XPS spectra of $[EMI^+][C_2H_5OSO_3^-]$ detailing the C1s photoemission (a) and those of $Pd(Oac)_2$ in $[EMI^+][C_2H_5OSO_3^-]$. The red line shows data recorded at the start of the XPs experiment and the black line presents data recorded 6 h later.

3. MALDI Mass Spectroscopy

The matrix-assisted laser desorption/ionization mass spectrometry (MALDI-MS) is one of the groundbreaking analysis techniques that vaporize samples by laser irradiation with assistance of an appropriate matrix, as schematically illustrated in Fig. 3(a). This way allows to vaporize very large molecules like proteins that could not been analyzed without decomposition of the sample by the conventional mass spectrometry. The Matrix selection is quite essential, and an ideal matrix is a material possessing sufficient absorption coefficient for the laser beam, low vapor pressure, ability to dissolve or co-crystallize with sample, and ability to promote ionization of sample without its significant decomposition. The liquid matrices having low vapor pressure like glycerol and 3-nitrobenzyl alcohol have been utilized in the early research but their inherent volatility still causes some problems, such as decrease in their amounts with time. Another problem is that these liquids possess no UV absorbability, requiring addition of another photosensitive component.

Since IL possesses both no volatility and UV absorbability, it seems to be an ideal solution matrix for MALDI. However, usual ILs such as $[BMI^+][BF_4^-]$ and $[BMI^+][PF_6^-]$ were unfortunately unable to ionize samples dissolved in them [15]. Then, new ionic liquid family for the liquid matrixes were synthesized using solid acidic compounds of α-cyano-4-hydroxycinnamic acid (CHCA), sinapinic acid (SA), and 2,5-dihydroxybenzoic acid (DHB), which are widely used as solid matrixes for MALDI-MS [15,16]. Then, some of them were found to keep liquid state at room temperature and work as liquid matrices for detection of polymer and some biomolecules by MALDI-MS [15-18].
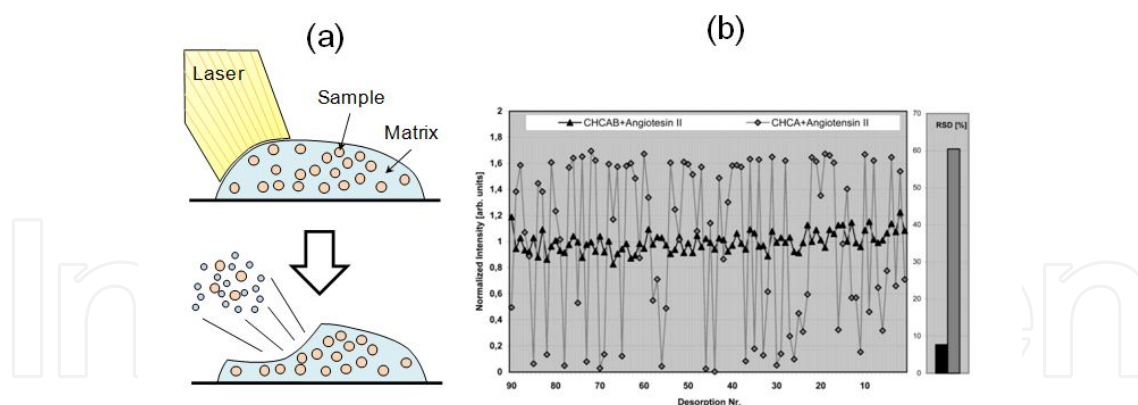
Figure 3. a) Schematic illustration of MALDI. (b) [M + H]+ ion intensities from 90 positions on a human angiotensin II preparation with ionic liquid matrix CHCAB (black triangles) and with traditional CHCA matrix (grey squares). The relative standard deviations (RSD) of the data series are given as bar graphs. Black bars indicate RSD values found using ionic liquid matrixes, and gray bars indicate RSD values of the data series yielded by the respective traditional MALDI matrixes.

Fig.3(b) shows change in signal intensities of [M + H]+ obtained at 90 different positions on a spot of sample-matrix mixture. As expected, the IL matrix of α-cyano-4-hydroxycinnamic acid butylamine (CHCAB) gave much narrow data dispersion than that obtained for the solid matrix of CHCA, indicating evidently usefulness of IL matrix for improvement of reproducibility. Another feature of the IL matrix is higher ability to suppress decomposition of sample than the conventional solid matrix. Use of CHCA-based guanidium salt and its analogous salts as IL matrixes enabled detection of oligosaccharides, which exhibit poor ionization efficiencies and tend to get thermal fragmentation through the loss of SO_3 groups, with suppression of loss of SO_3 [17,18].

4. Use of ILs for SEM observations

The first attempt was to observe ILs with a scanning electron microscope (SEM) [19]. The fact that ILs possess ionic conductivity but they do not possess electric conductivity gave an anticipation of charging of a IL drop during SEM observation. As a matter of fact, nonvolatile silicon oil, which can also be put in a vacuum chamber without vaporization, exhibited a white image with lots of noise because of charging behavior (Fig. 4(a)). Surprisingly, however, IL droplet gave a dark contrast images without any noise (Figure 4(b) -(d)), indicating that ILs are not charged by electron beam irradiation. Pulse radiolysis studies on ILs have revealed that electrons injected in ILs with high accelerated voltage are stabilized in condensed ions, allowing electrons to move in the liquid [20]. Consequently, ILs behave like electrically conducting materials for SEM observations. Based on this fact, several attempts have been done for SEM observations using ILs. The simplest way must be putting conductivity in place of metal or carbon deposition to insulating materials to observe them with a SEM. However, if neat IL was put onto the surface of the insulating material, existence of the

liquid pools interfered observations of surface details of the abrasive paper, as shown in Fig. 5 (b), as compared with the case of the Au-deposited sample (Fig. 5 (a)). This troublesome can be resolved by dilution of IL with volatile solvent like alcohol. The abrasive paper was soaked in 2 mol dm^{-3} [BMI$^+$][TFSA$^-$] / ethanol solution in a couple of seconds and was taken out of the solution. Leaving it in air for several ten seconds allowed vaporization of ethanol, resulting in stay of a thin IL layer on the sample. In fact, its SEM image as shown in Fig. 5c was quite similar to that obtained for the Au-coated abrasive paper [21].
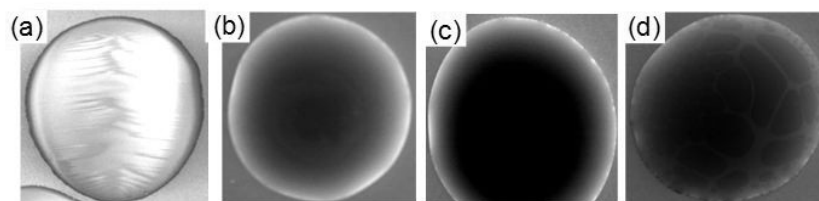

Figure 4. SEM images of droplets of silicon oil (a), [BMI$^+$][BF$_4^-$] (b), [EMI$^+$][BF$_4$] (c), and [EMI$^+$][TFSA$^-$]
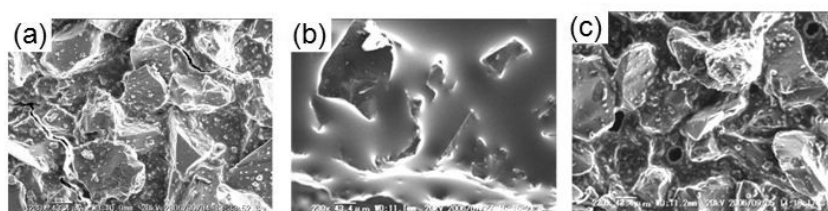

Figure 5. SEM images of surfaces of abrasive paper coated with gold (a), neat [BMI$^+$][TFSA$^-$] (b), and /ethanol solution (c).
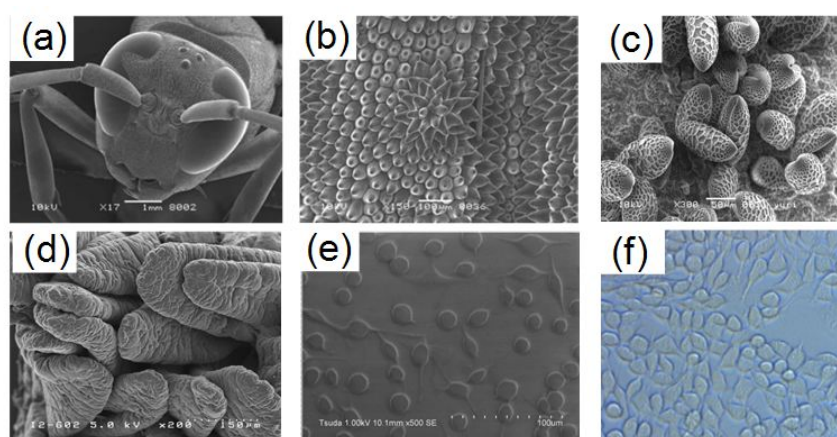

Figure 6. SEM images of insect, flower, tissue, and cell pretreated with IL; a) head of a yellow jacket, b) stamen of asteraceae, c) pollens of lily, d) villi of mouse small intestine, and mouse-derived fibroblast L929 cells (e). A picture (f) is optical microscope image of L929 cells for comparison.

Application of IL as an electric conducting material to an insulating sample gives another advantages, as compared with metal or carbon deposition. The liquid can keep the sample wet conditions even in vacuum chamber. This possibility has in particular a positive effect on observation of biological specimens [22-25]. Some examples are shown in Fig. 6 [22]. Since biological specimens have complex surface structures, metal or carbon deposition cannot perfectly deposit conducting films on the surfaces having dimples and indented places. However, liquid can reach anywhere on the complex surfaces, resulting in complete suppression of the charging behavior. Also replacement of water contained in the biological specimens with IL keeps the sample wet condition. As a result, SEM image of IL-treated fibrous blast cells, as shown in Fig. 6(e) was quite similar to shapes of cells containing water, which were observed by an optical microscope (Fig. 6(f)).

The IL treatment became now significant for biological and medical studies by electron microscope observations. An example is shown in Fig. 7 [23,24]. The metastasis is one of the most serious problems during cancer treatment. Such action has never been seen for the normal cells which prefer to adhere to each other during and after the cell fissions. This means that the normal cells must have some specific means to keep connections with neighboring cells. It is already known that something works well to make cell-to-cell junction, but direct observation of the something by an electron microscope has not yet been succeeded.
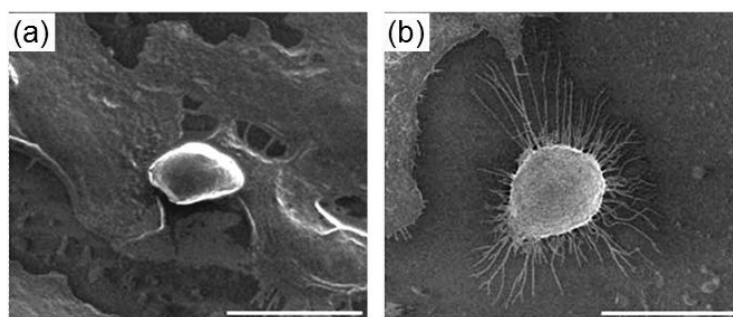

Figure 7. SEM images of A549 cells with (a) and without (b) pre-TGF-β1 treatment for 18 h. The IL treatment was conducted for the both samples before SEM observation.

The cells shown in Fig. 7 are human lung epithelial cells (A549). Before SEM observation of the cells, fixation treatment and metal or carbon coating are required to keep the cell morphology under vacuum conditions and to put electrical conductivity. Sometimes, however, such the treatments deform the delicate moieties of the cells. The A549 cells, which were subjected to dehydration and Pt-sputtering gave their SEM images showing relatively smooth surface with short microvilli. On the other hand, if IL was applied to the cells in place of the Pt-sputtering to put electrical conductivity to the cell, the SEM image shown in Fig. 7(b) was obtained. It indicates evidently long microvilli around the cell and ruffled cell surface. It is noteworthy that some of long microvilli made connections between separated cells, forming cellular bridges. The transforming growth factor (TFG)-β1 is a representative epthelial-mesenchymal transition (EMT), which is a key event in cancer metastasis. In fact, it is well known that the cells pre-treated with (TFG)-β1 lose their polarity and cell-to-cell con-

tact. Fig. 7(a) shows A549 cells, which were subjected to the (TFG)-β1 treatment before SEM observation using IL. It is apparent by comparison of Fig. 7(a) with (b) that the A549 treated with (TFG)-β1 completely lost microvilli, implying that EMT-inducing TGF- β1 on the regulation of filopodia formation in mitotic cells. As a result the cells, which are free from other cells, enable their metastases.

5. Observation of electrochemical reactions

ILs work as a favorable electrolyte for several kinds of electrochemical reactions, implying that such the electrochemical reactions can be induced in a vacuum chamber, allowing observation of the reactions by an electron microscope [26,27]. As the first attempt, SEM observation of electrochemical Ag deposition has been conducted. Since the electrochemical reaction proceeds in IL as an electrolyte, IL may disturb the observation. However, the reaction occurring at several μm from the IL surface can be observed because the accelerated electron beam of SEM can penetrate such a thing IL layer.

In situ SEM observation of silver deposition was made by applying electrode potential to the working electrode, while observing the electrode surface from the top. The polarization potential chosen was -0.22 V, which was a little more negative than the onset potential of silver deposition (-0.15 V), and -1.14 V vs. Ag/Ag$^+$ where the reaction rate is determined by diffusion of Ag$^+$. It is well known that silver deposition with nucleus growth is dominant when overpotential is small, whereas aciculate deposits becomes dominant at the potentials where diffusion determines the reaction rate. Such the natural rule was well represented by the SEM images taken with the reaction time, as shown in Fig. 8 [26].
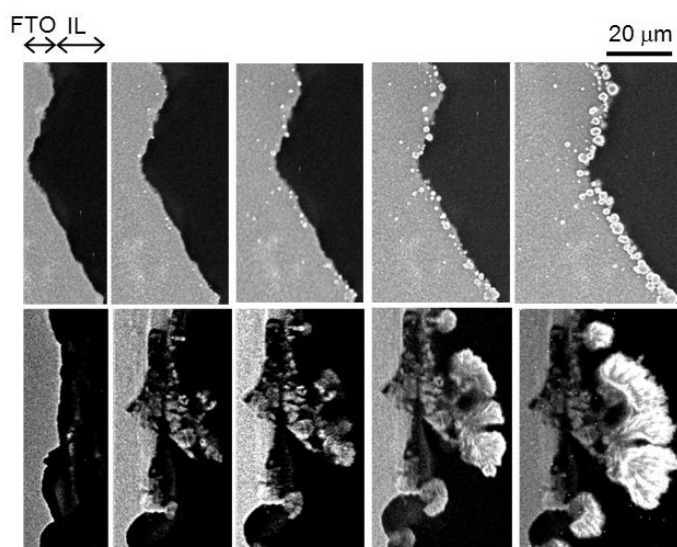

Figure 8. SEM images of gradual deposition of silver particles polarized at 0.22 V (upper) and -1.14 V (lower) vs. Ag/Ag$^+$ for 0, 15, 30, 60 min, and180 min.

6. EDX analysis

Energy dispersive X-ray spectrometry (EDX) has become powerful for elemental analysis at small parts when it is combined with electron microscopes. Our previous studies revealed that EDX analysis is effective for detecting changes in components caused by electrochemical reactions in ILs. As a concrete application, we utilized this technique to reveal reaction mechanism of the electrochemical actuator.

The actuator device was prepared using a film of poly(vinylidene fluoride-co-hexafluoropropylene) (PVdF-HFP) containing IL. This composite film was sandwitched between two thin Au or Pt layers that were deposited by a metal sputtering. When [EMI⁺][TFSA⁻] was used to prepare the PVDF-HFP-IL composite, the resulting actuator bent toward the positive side (Fig. 10 (a)). The same tendency was observed for other polymer-IL composite actuators. Based on such the results, some researchers explained that bending is caused by difference in size between cation and anion of IL, the former is a little larger than the latter. Therefore, larger cations and smaller anions are attracted to the negative and the positive metal layer, respectively, resulting in expansion of the former side more than the latter.
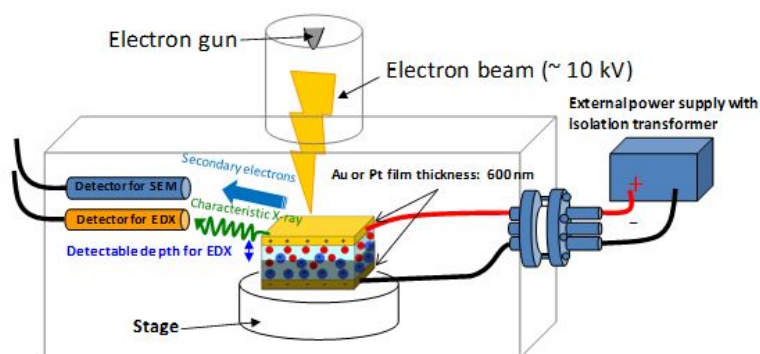

Figure 9. Schematic illustration of in situ SEM system for an actuator to investigate component changes by its reaction.

However, unexpected result was obtained when the fluorohydrogenate IL, [EMI⁺][(FH)$_{2.3}$F⁻] was used for the composite preparation. The actuator fabricated using this composite bent toward its negative side, as shown in Fig. 10 (b) although size of [(FH)$_{2.3}$F⁻] is smaller than [TFSA⁻], requiring another reaction mechanism that can explain reasonably the bending toward positive and negative sides. Then, we attempted in situ EDX analysis using the specifically modified SEM instrument, as shown in Fig. 9.

The prepared actuator was put on the sample stage of the SEM and DC voltage of + 3.5 V was applied to the Pt layers from a power supply outside of the SEM chamber. The one side of the actuator was observed by the SEM and change in amount of ions at vicinity of the Pt layer was detected by EDX while changing polarity of the DC supply. Typical change in the EDX spectra were shown in Fig. 10 (c) and (d). In case of the [EMI⁺][TFSA⁻] composite, the peak intensities for the anion components such as O, F, and S did not show significant change at all after changing polarity, while the intensity of carbon, which is mainly con-

tained in the cation, markedly increased when the polarity was changed from plus to minus. On the contrary, in case of the [EMI⁺][(FH)$_{2.3}$F⁻] composite, the F intensity decreased by changing voltage from +3.5 to -3.5 V, while almost no change was observed for the carbon intensity. Such the results indicated that cations and anions moved dominantly by changing the voltage polarity. Those behavior may be comprehensible because the transport numbers of cations and anions are larger for [EMI⁺][TFSA⁻] and [EMI⁺][(FH)$_{2.3}$F⁻], respectively. Based on those results and information, schematic illustrations shown in Fig. 10 (e) and (f) can be depicted to explain the actuator's bending. If only cations move in the polymer-IL composite, population of ions existing in the vicinity of the positive side decreases and that in the vicinity of the negative side increases, resulting in bending toward the positive side. It is, therefore, explainable that the bending toward the negative side in case of the IL, anion of which has larger transport number than cation, as shown in Fig. 10 (f) [28].
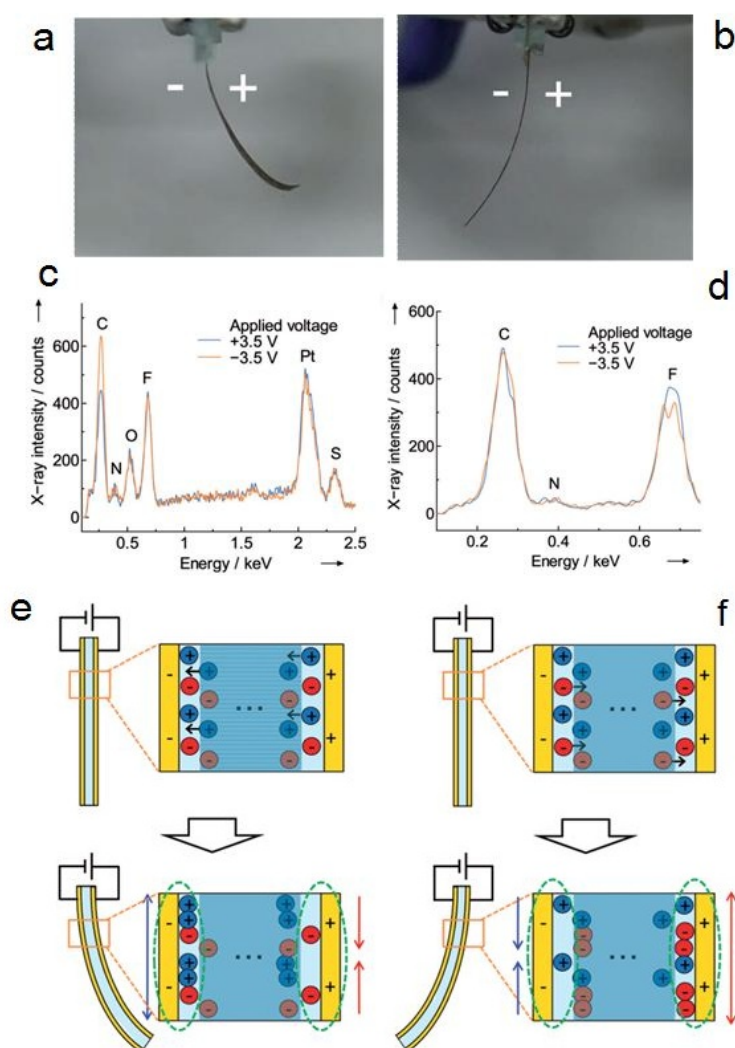

Figure 10. Motion of the electrochemical actuators prepared using ILs of [EMI⁺][TFSA⁻] (a) and [EMI⁺][(FH)$_{2.3}$F⁻] (b), their in situ EDX results (c, d), and plausible reaction mechanisms (e, f).

7. Preparation of metal nanoparticles by plasma deposition method

Ag, Cu, and Al nanoparticles have been successfully synthesized by plasma deposition method [29-31]. This approach called glow discharge electrolysis, is based on historical articles reported about 100 years ago. Schematic illustration of the system for the plasma deposition is illustrated in Fig. 11 (a). The plasma generation does not need vacuum conditions, but appropriate gas of low pressure is required to generate a stable plasma. However, the use of ILs is also essential in this case because the presence of vapor of a volatile liquid in the gas phase would inhibit the plasma generation. A typical plasma experiment is shown in Fig. 11 (b) [31]. The reaction media was [EMI$^+$][TFSA$^-$] with 62 mmol L^{-1}Cu(I). A dark brown-layer that appeared at the interphase between the IL and plasma phase was growing with plasma irradiation time, indicating that Cu(I) was reduced to Cu nanoparticles with an average size of ~11 nm. However, the surface was covered with a copper oxide layer. If the metal nanoparticles are yielded under vacuum or inert gas condition, this is a common issue for which it is very difficult to collect metallic state nanoparticles, especially base metal nanoparticles that are oxidized readily under atmospheric condition. One of solution methodologies about this will be introduced in a later section. Very recently, the plasma deposition method was adopted for preparation of Au [32,33] and Pt [33] nanoparticles. The relationship between deposition conditions and the characteristics of the prepared nanoparticles was studied in detail. One of interesting findings is that nanoparticles were prepared even if the cathode was placed in the IL phase and not the gas phase.
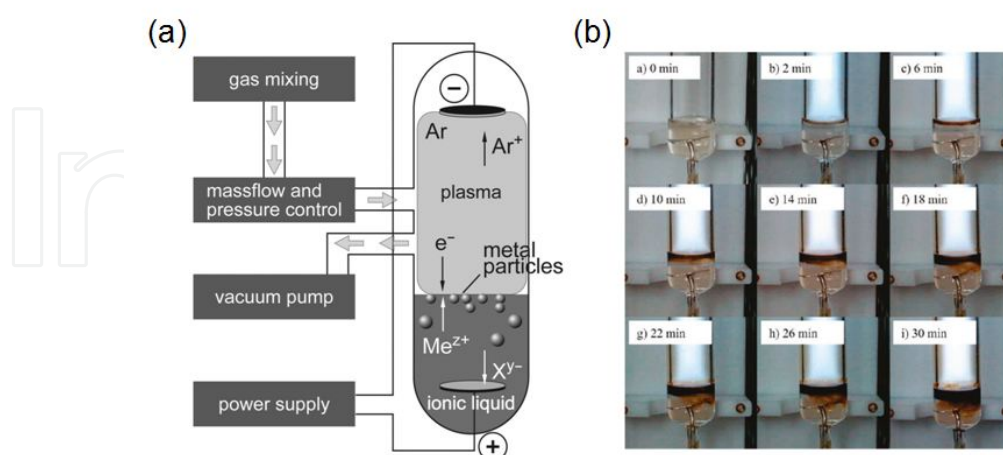

Figure 11. Schematic illustration of the experimental setup for plasma electrochemical reduction of metal ions dissolved in ILs (a) and photographs of the plasma electrochemical reduction experiment of Cu(I) dissolved in a IL at different reduction times (b).

8. Nanoparticle synthesis by sputtering

It is well known that metal vapor-deposition is a method to prepare ultrapure metal nanoparticles or films on solid substrates. Several research groups have developed the sputter deposition of metal nanoparticle onto pure ILs, as schematically illustrated in Fig. 12 (a), in order to prepare ultrapure metal nanoparticles [32-38]. The simple sputter deposition of Au onto ILs resulted in a solution containing highly dispersed Au nanoparticles whose size was dependent on the IL used [32]. In situ TEM observations of Au-deposited ILs revealed that highly-dispersed nanoparticles with no aggregation were seen in ILs, as shown in Fig. 12 (b), (c). Sputter deposition onto $[EMI^+][BF_4{}^-]$ gave spherical Au nanoparticles having an average diameter of 5.5 nm, while much smaller nanoparticles with size of 1.9 nm were obtained for the experiment using $[Me_3PrN^+][TFSA^-]$. Although sputtered species were assumed not to considerably suffer gas-phase collisions in the space between Au foil and IL solution because of low gas pressure, their injection into IL solution could make high concentration enough to coalesce with each other. Their coalescence would proceed until Au nanoparticles were stabilized by the adsorption of IL ions, the degree being dependent on IL. Since it is well-known that $TFSA^-$ anion makes a coordination bond with metal ions, it is expected that strong adsorption of $TFSA^-$ suppresses the growth and/or coalescence of particles.
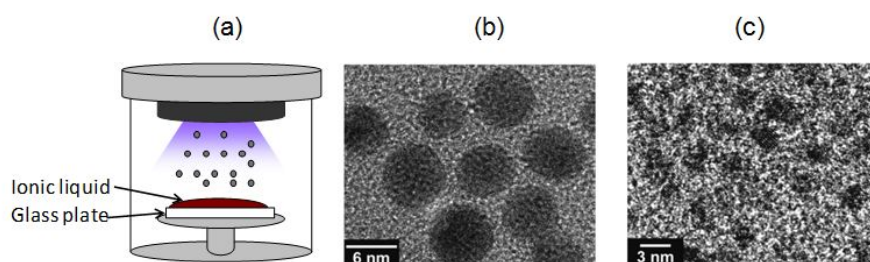

Figure 12. Schematic illustration of the metal nanoparticle formation by sputtering (a) and TEM image of Au nanoparticles sputter-deposited in $EtMeImBF_4$.

This method has achieved the preparation of various pure metal nanoparticles, such as Au [32-36], Ag [37,38], Pt [39,40] and so forth, possessing particle sizes less than 10 nm in diameter without any specific stabilizing agent. A small-angle X-ray scatting study revealed the initial formation mechanism of the gold nanoparticles during the sputtering process onto several [1,3-dialkylimidazolium][BF_4] [36]. The proposed formation mechanism is divided into two phases where it was concluded that both surface tension and viscosity of the IL are important factors for the Au nanoparticle growth and its stabilization.

The simultaneous sputter deposition of different pure metals on IL is a facile synthetic method to prepare bimetallic alloy nanoparticles [37]. The use of metal targets composed of radially-arranged Au and Ag foils allowed simultaneous sputter deposition of Au and Ag onto $[BMI^+][PF_6{}^-]$ in argon atmosphere at ca. 20 Pa. The color of $[BMI^+][PF_6{}^-]$ subjected to the sputter deposition was varied (Fig. 11), depending on a fraction of gold foils on targets. Each absorption spectrum of the resulting solution exhibited a single peak or shoulder assigned

to the surface plasmon resonance (SPR) band of the metal particles and the peak wavelength increased almost linearly with the Au fraction. These results indicated that the simultaneous injection of sputtered species of Au and Ag into an IL caused coalescence with each other in the solution, resulting in the formation of AuAg alloy nanoparticles, as shown in Fig. 13. The chemical composition and optical properties of the alloy nanoparticles are easily controlled just by varying the area ratio of the individual pure metal foils in a sputtering target.
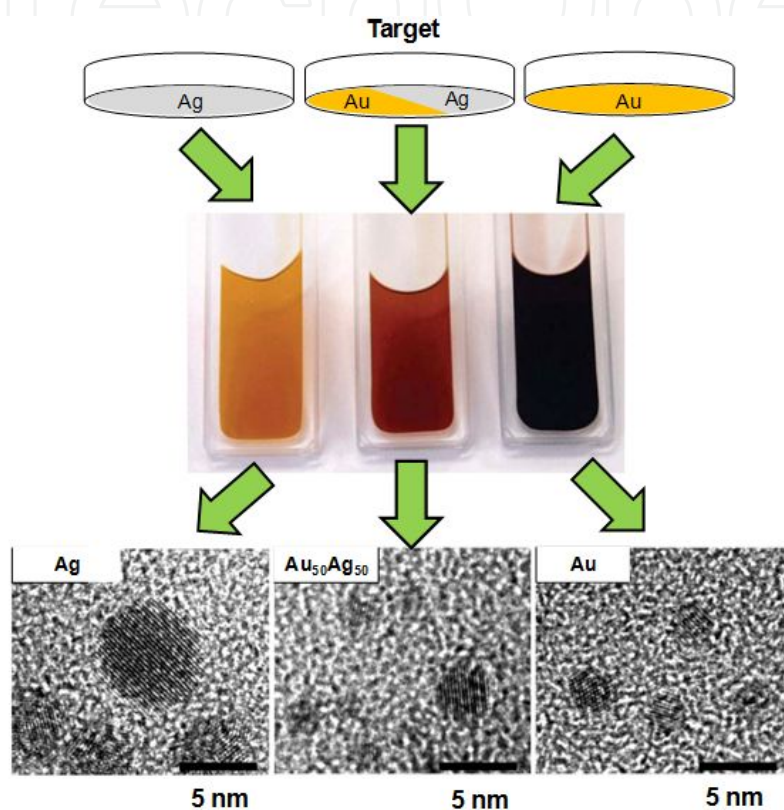

Figure 13. Photographs of [BuMeIm][PF$_6$] ILs after sputtering experiments at Au-Ag targets having different surface area ratios and TEM images of the resulting nanoparticles obtained at each Au-Ag target.

Furthermore, it was discovered that hollow nanoparticles can be synthesized by some modification of the sputtering method [39]. This fact was found when we attempted to produce indium metal nanoparticles by sputtering of In onto [BMI$^+$][BF$_4$ $^-$]. SEM observation and some analyses of the obtained nanoparticles revealed that they had In/In$_2$O$_3$ core/shell configuration, as shown in Fig. 14(a). Since the melting point of In is 156.6 $^\circ$C, we attempted to heat the resulting In/In$_2$O$_3$-dispersed IL at 250 $^\circ$C, giving the In$_2$O$_3$ hollow nanoparticles, a TEM image of which is shown in Fig. 14(b). The plausible reaction mechanisms for synthesis of In/In$_2$O$_3$ and In$_2$O$_3$ hollow nanoparticles are schematically illustrated in Fig. 12(c) and (d), respectively. The oxidation of the In nanoparticle surfaces and the melted In by heating might be caused by oxygen that was dissolved in the IL when the IL was taken out from the sputtering instrument.
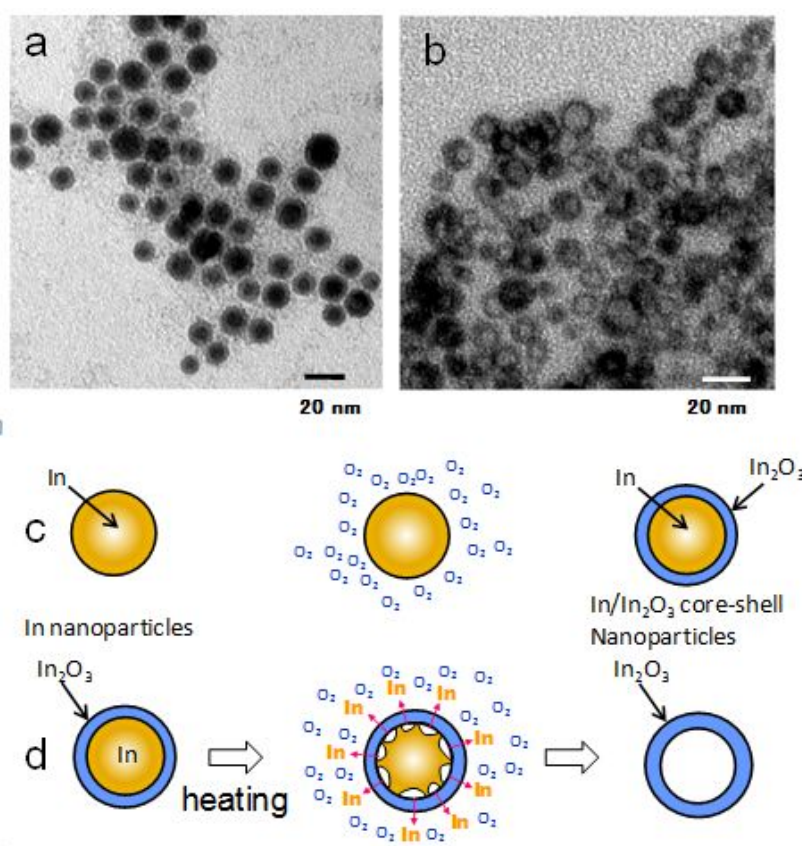
Figure 14. Nanoparticles synthesized by sputtering of In onto [EMI⁺][BF₄⁻] (a), those after heating at 250 °C, and the plausible reaction mechanisms for the In sputtering (c) and the heating (d) procedures.
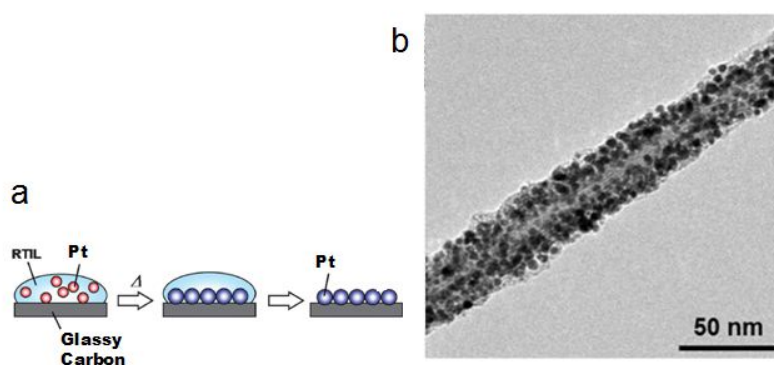
Figure 15. A way to immobilize Pt nanoparticles on surface of carbon substance (a) and Pt nanoparticles-immobilized carbon nanotube (b) prepared by this way.

The produced metal nanoparticles are stably dispersed in ILs for long time without any specific stabilizing agent. However, the nanoparticles can be immobilized onto carbon substances by putting the nanoparticles-dispersed IL on a carbon substrate followed by heating and then removal of IL by washing with acetonitrile (Fig. 15(a)) [34]. When the resulting Pt nano-

particles-immobilized carbon substance was used as an electrode, it exhibited high electro-catalytic activities toward O_2 reduction, indicating that the immobilized Pt nanoparticles kept their catalytic acitvities [40,41]. Similar method was found to be useful to immobilize Pt nanoparticles onto surfaces of carbon nanotubes, as shown in Fig. 15 (b) [42]. In this case, Pt-dispersed IL and carbon nanotubes are vigorously mixed and the resulting mixture was heated, followed by washing with acetonitrile. The Pt nanoparticles on the carbon nanotubes also exhibited high electrocatalytic activities, as shown in Fig. 14.
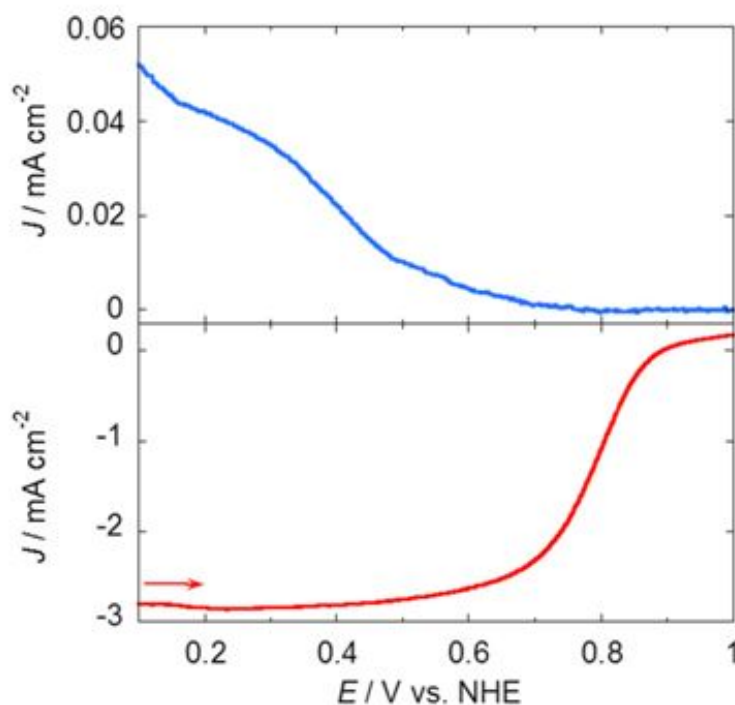

Figure 16. Hydrodynamic voltammograms for O_2 reduction at a Pt–SWCNT modified rotating ring disk electrode in O_2-saturated 0.1 M $HClO_4$ aqueous solution at 298 K. The electrodes were (top) Pt ring and (bottom) Pt–SWCNT modified GC disk. The IL used for Pt nanoparticle preparation was [Me_3PrN^+][$TFSA^-$]. The potential for the ring electrode was 1.20 V. The scan rate was 10 mV s^{-1}; the rotation rate was 1200 rpm.

9. Nanoparticle preparation by quantum Beam

Irradiation of electron beam to IL is another way to synthesize metal particles. This fact was found first when we observed [BMI^+][$TFSA^-$] containing 0.1 mol dm^{-3} $NaAuCl_4$ [43]. As shown in Fig. 17(a)-(c), many bright lines appeared in the IL droplet on a FTO with observation time. When the bright line was observed with higher magnification, a SEM image of Fig. 17 (d) was obtained, showing Several experiments and analyses have revealed that Au particles are produced by reduction of Au^{3+} ions by electron beam, and that particle size depends on the experimental conditions [44].
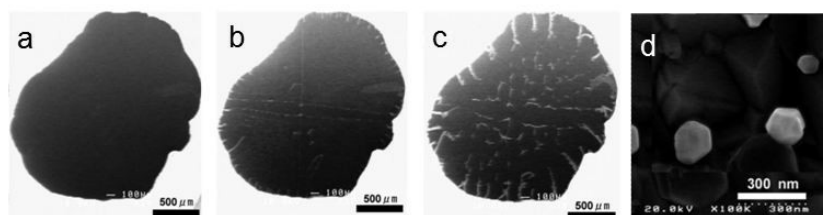
Figure 17. SEM images of the ionic liquid irradiated with an electron beam for 0 s (a), 90 s (b), and 300 s (c), and generated Au particles (d).

Accelerated electron beam and γ-ray generated by industrial plants, which are usually utilized for sterilizing medical kits, are also available for reduction of metal ions to metal nanoparticles [45]. In this case, since irradiation is made by conveying IL containing metal ions, which is sealed in a sample vial, through the generator, mass production of metal nanoparticles is possible. This technique was able to synthesize several kinds of metal nanoparticles, such as Au, Ag, Cu, Ni, Pd, Pt, Mg, Fe, Zn, Al, Sn, and FePt alloy [46].

10. Conclusion Remarks

Chemists prefer wet conditions than dry conditions because wet conditions are more desired for inducing chemical reactions. Since wet conditions are also required for all living things, investigation of biomaterials under wet conditions are much better than that under dry conditions. Unfortunately, however, many instruments for precise analyses and those for material production with micro or nano scales require vacuum conditions because the air intererferes precise proving and controlling. So far, vacuum and wet are contradictory words because there is no liquid which can stand in vacuum without vaporization. IL is the first liquid that can set the relationship between vacuum and wet on the right footing. There are more instruments requiring vacuum conditions than those introduced in this article. We would like to apply IL to more instruments to make many scientists know that IL is the key material to solve the mysteries of our wet world.

Author details

Susumu Kuwabata[1,2], Tsukasa Torimoto[2,3], Akihito Imanishi[2,4] and Tetsuya Tsuda[1,4]

*Address all correspondence to: kuwabata@chem.eng.osaka-u.ac.jp

1 Department of Applied Chemistry, Graduate School of Engineering, Osaka University, Japan

2 Japan Science and Technology Agency, CREST, Japan

3 Department of Crystalline Material Sciences, Graduate School of Engineering, Nagoya University, Japan

4 Department of Chemistry, Graduate School of Engineering Science, Osaka University, Japan

Frontier Research Base for Global Young Researchers, Graduate School of Engineering, Japan

References

[1] Ohno, H. (2005). Electrochemical Aspects of Ionic Liquids. *Wiley-Interscience, New Jersey*.

[2] Wasserscheid, P., & Welton, T. (2007). Ionic Liquids in Synthesis. *Wiley-VCH, Weinheim, Germany*.

[3] Koel, M. (2009). Ionic Liquids in Chemical Analysis. *CRC Press, Boca Raton*.

[4] Torimoto, T., Tsuda, T., Okazaki, K. I., & Kuwabata, S. (2010). New Frontiers in Materials Science Opened by Ionic Liquids. *Adv. Mater*, 22(5), 1196-1221.

[5] Kuwabata, S., Tsuda, T., & Torimoto, T. (2010). Room-Temperature Ionic Liquid. A New Medium for Material Production and Analyses under Vacuum Conditions. *J. Phys. Chem. Lett.*, 1(21), 3177-3188.

[6] Oliveira, F. C. C., Rossi, L. M., Jardim, R. F., & Rubim, J. C. (2009). Magnetic Fluids Based on γ-Fe$_2$O$_3$ and CoFe$_2$O$_4$ Nanoparticles Dispersed in Ionic Liquids. *J. Phys. Chem. C*, 113(20), 8566-8572.

[7] Swatloski, R. P., Spear, S. K., Holbrey, JD, & Rogers, R. D. (2002). Dissolution of cellose with ionic liquids. *J. Am. Chem. Soc.*, 124(18), 4974-4975.

[8] Zhu, S., Wu, Y., Chen, Q., Yu, Z., Wang, C., Jin, S., Ding, Y., & Wu, G. (2006). Dissolution of cellulose with ionic liquids and its application: a mini-review. *Green Chem*, 8(4), 325-327.

[9] Feng, L., & Chen, Z. (2008). Research progress on dissolution and functional modification of cellulose in ionic liquids. *J. Mol. Liq*, 142(1-3), 1-5.

[10] Smith, E. F., Rutten, F. J. M., Villar-Garcia, I. J., Briggs, D., & Licence, P. (2006). Ionic Liquids in Vacuo: Analysis of Liquid Surfaces Using Ultra-High-Vacuum Techniques. *Langmuir*, 22(22), 9386-9392.

[11] Hofft, O., Bahr, S., Himmerlich, M., Krischok, S., Schaefer, J. A., & Kempter, V. (2006). Electronic Structure of the Surface of the Ionic Liquid [EMIM][Tf$_2$N] Studied by Metastable Impact Electron Spectroscopy (MIES), UPS, and XPS. *Langmuir*, 22(17), 7120-7123.

[12] Caporali, S., Bardi, U., & Lavacchi, A. (2006). X-ray Photoelectron Spectroscopy and Low Energy Ion Scattering Studies on 1-Butyl-3-methyl-imidazolium Bis(Trifluoro-methane) Sulfonamide. *J. Electron Spectrosc. Relat. Phenom*, 151(1), 4-8.

[13] Lovelock, K. R. J., Kolbec, C., Cremer, K. T., Paape, N., Schulz, P. S., Wasserscheid, P., Maier, F., & Steinruck, H. P. (2009). Influence of Different Substituents on the Surface Composition of Ionic Liquids Studied Using ARXPS. *J. Phys. Chem. B*, 113(9), 2854-2864.

[14] Smith, E. F., Villar, Garcia. I. J., Briggs, D., & Licence, P. (2005). Ionic Liquids in Vacuo; Solution-Phase X-ray Photoelectron Spectroscopy. *Chem. Commun*, 5633-5635.

[15] Armstrong, D. W., Zhang, L. K., He, L., & Gross, M. L. (2001). Ionic Liquids as Matrixes for Matrix-Assisted Laser Desorption/Ionization Mass Spectrometry. *Anal. Chem*, 73(15), 3679-86.

[16] Mank, M., Stahl, B., & Boehm, G. (2004). Dihydroxybenzoic Acid Butylamine and Other Ionic Liquid Matrixes for Enhanced MALDI-MS Analysis of Biomolecules. *Anal. Chem*, 76(10), 2938-2950.

[17] Laremore, T. N., Zhang, F., & Linhardt, R. J. (2007). Ionic Liquid Matrix for Direc UV-MALDI-TOF-MS Analysis of Dermatan Sulfate and Chondroitin Sulfate Oligosaccharides. *Anal. Chem.*, 79(4), 1604-1610.

[18] Fukuyama, Y., Nakaya, S., Yamazaki, Y., & Tanaka, K. (2008). Ionic Liquid Matrixes Optimized for MALDI-MS of Sulfated/Sialylated/Neutral Oligosaccharides and Glycopeptides. *Anal. Chem*, 80(6), 2171-2179.

[19] Kuwabata, S., Kongkanand, A., Oyamatsu, D., & Torimoto, T. (2006). Observation of Ionic Liquid by Scanning Electron Microsocope. *Chem. Lett*, 35(6), 600-601.

[20] Wishart, J. F., & Neta, P. (2003). Spectrum and Reactivity of the Solvated Electron in the Ionic Liquid Methyltributylammonium Bis(trifluoromethylsulfonyl)imide. *J. Phys. Chem. B.*, 107(30), 7261-7267.

[21] Arimoto, S., Sugimura, M., Kageyama, H., Torimoto, T., & Kuwabata, S. (2008). Development of New Techniques for Scanning Electron Microscope Observation Using Ionic Liquid. *Electrochim. Acta*, 53(21), 6228-6234.

[22] Tsuda, T., Nemoto, N., Kawakami, K., Mochizuki, E., Kishida, S., Tajiri, T., Kushibiki, T., & Kuwabata, S. (2011). SEM Observation of Wet Biological Specimens Pretreated with Room-Temperature Ionic Liquid. *ChemBioChem*, 12(17), 2547-2550.

[23] Ishigaki, Y., Nakamura, Y., Takehara, T., Nemoto, N., Kurihara, T., Koga, H., Nakagawa, H., Takegami, T., Tomosugi, N., Miyazawa, S., & Kuwabata, S. (2011). Ionic liquid enables simple and rapid sample preparation of human culturing cells for scanning electron microscope analysis. *Microsc. Res. Tech*, 74(5), 415-420.

[24] Ishigaki, Y., Nakamura, Y., Takehara, T., Shimasaki, T., Tatsuno, T., Takano, F., Ueda, Y., Motoo, Y., Takegami, T., Nakagawa, H., Kuwabata, S., Nemoto, N., Tomosugi, N.,

& Miyazawa, S. (2011). Scanning electron microscopy with an ionic liquid reveals the loss of mitotic protrusions of cells during the epithelial-mesenchymal transition. *Microsc. Res. Tech*, 74(11), 1024-1031.

[25]   Yanaga, K., Maekawa, N., Shimomura, N., Ishigaki, Y., Nakamura, Y., Takegami, T., Tomosugi, N., Miyazawa, S., & Kuwabata, S. (2012). Use of ionic liquid in fungal taxonomic study of ultrastructure of basidiospore ornamentation. *Mycolog. Prog.*, 11(1), 343-347.

[26]   Arimoto, S., Kageyama, H., Torimoto, T., & Kuwabata, S. (2008). Development of In Situ Scanning Electron Microscope System for Real Time Observation of Metal Deposition from Ionic Liquid. *Electrochem. Commun*, 10(12), 1901-1904.

[27]   Arimoto, S., Oyamatsu, D., Torimoto, T., & Kuwabata, S. (2008). Development of in situ electrochemical scanning electron microscopy with ionic liquids as electrolytes. *Chem Phys Chem*, 9(5), 763-767.

[28]   Tsuda, T., Baba, M., Sato, T., Sakao, R., Matsumoto, K., Hagiwara, R., & Kuwabata, S. (2011). Nonvolatile IL-based artificial muscle: Actuation mechanism identified by in situ EDX analysis. *Chem. Europ. J.*, 17(40), 11122-11126.

[29]   Meiss, S. A., Rohnke, M., Kienle, L., Abedin, S. E., Endres, F., & Janek, J. (2007). Employing Plasmas as Gaseous Electrodes at the Free Surface of Ionic Liquids: Deposition of Nanocrystalline Silver Particles. *ChemPhysChem*, 8(1), 50-3.

[30]   Abedin, S. Z. E., Pölleth, M., Meiss, S. A., Janek, J., & Endres, F. (2007). Ionic Liquids as Green Electrolytes for the Electrodeposition Nanomaterials. *Green Chem.*, 9(6), 549-553.

[31]   Brettholle, M., Höfft, O., Klarhöfer, L., Mathes, S., Friedrichs, M., Abedin, S. Z. E., Krischok, S., Janek, J., & Endres, F. (2010). Plasma electrochemistry in ionic liquids: deposition of copper nanoparticles. *Phys. Chem. Chem. Phys.*, 12(8), 1750-1755.

[32]   Torimoto, T., Okazaki, K., Kiyama, T., Hirahara, K., Tanaka, N., & Kuwabata, S. (2006). Sputter Deposition onto Ionic Liquids: Simple and Clean Synthesis of Highly Dispersed Ultrafine Metal Nanoparticles. *Appl. Phys. Lett*, 89(24), 243117/1-243117/3.

[33]   Khatri, O. P., Adachi, K., Murase, K., Okazaki, K., Torimoto, T., Tanaka, N., Kuwabata, S., & Sugimura, H. (2008). Self-Assembly of Ionic Liquid (BMI-PF$_6$)-Stabilized Gold Nanoparticles on a Silicon Surface: Chemical and Structural Aspects. *Langmuir*, 24(15), 7785-7792.

[34]   Okazaki, K., Kiyama, T., Suzuki, T., Kuwabata, S., & Torimoto, T. (2009). Thermally Induced Self-assembly of Gold Nanoparticles Sputterdeposited in Ionic Liquids on Highly Ordered Pyrolytic Graphite Surfaces. *Chem. Lett.*, 38(4), 330-331.

[35]   Kameyama, T., Ohno, Y., Kurimoto, T., Okazaki, K., Uematsu, T., Kuwabata, S., & Torimoto, T. (2010). Size Control and Immobilization of Gold Nanoparticles Stabilized in an Ionic Liquid on Glass Substrates for Plasmonic Applications. *Phys. Chem. Chem. Phys.*, 12(8), 804-811.

[36] Hatakeyama, Y., Okamoto, M., Torimoto, T., Kuwabata, S., & Nishikawa, K. (2009). Small-Angle X-ray Scattering Study of Au Nanoparticles Dispersed in the Ionic Liquids 1-Alkyl-3-methylimidazolium Tetrafluoroborate. *J. Phys. Chem. C*, 113(10), 3917-3922.

[37] Okazaki, K., Kiyama, T., Hirahara, K., Tanaka, N., Kuwabata, S., & Torimoto, T. (2008). Single-Step Synthesis of Gold-Silver Alloy Nanoparticles in Ionic Liquids by a Sputter Deposition Technique. *Chem. Commun*, 691-693.

[38] Suzuki, T., Okazaki, K., Kiyama, T., Kuwabata, S., & Torimoto, T. (2009). A Facile Synthesis of AuAg Alloy Nanoparticles Using a Chemical Reaction Induced by Sputter Deposition of Metal onto Ionic Liquids. *Electrochemistry*, 77(8), 636-638.

[39] Suzuki, T., Okazaki-I, K., Suzuki, S., Shibayama, T., Kuwabata, S., & Torimoto, T. (2010). Nanosize-controlled syntheses of indium metal particles and hollow indium oxide particles via the sputter deposition technique in ionic liquids. *Chem. Mater.*, 22(18), 5209-5215.

[40] Tsuda, T., Kurihara, T., Hoshino, Y., Kiyama, T., Okazaki-I, K., Torimoto, T., & Kuwabata, S. (2009). Electrocatalytic activity of platinum nanoparticles synthesized by room-temperature ionic liquid-sputtering method. *Electrochemistry*, 77(8), 693-695.

[41] Tsuda, T., Yoshii, K., Torimoto, T., & Kuwabata, S. (2010). J. Power Sources , 195, 5980-5985.

[42] Yoshii, K., Tsuda, T., Arimura, T., Imanishi, A., Torimoto, T., & Kuwabata, S. (2012). Platinum nanoparticle immobilization onto carbon nanotubes using Pt-sputtered room-temperature ionic liquid. *RSC Adv*, 10.1039/C2RA21243A.

[43] Imanishi, A., Tamura, M., & Kuwabata, S. (2009). Formation of Au nanoparticles in an ionic liquid by electron beam irradiation. *Chem. Commun*, 1775-1777.

[44] Imanishi, A., Gonsui, S., Tsuda, T., Kuwabata, S., & Fukui-I, K. (2011). Size and shape of Au nanoparticles formed in ionic liquids by electron beam irradiation. *Phys. Chem. Chem. Phys.*, 13(33), 14823-14830.

[45] Tsuda, T., Seino, S., & Kuwabata, S. (2009). Gold nanoparticles prepared with a room-temperature ionic liquid-radiation irradiation method. *Chem. Comm*, 6792-6794.

[46] Tsuda, T., Sakamoto, T., Nishimura, Y., Seino, S., Imanishi, A., & Kuwabata, S. (2012). Various metal nanoparticles produced by accelerated electron beam irradiation of room-temperature ionic liquid. *Chem. Commun.*, 925-927.